

IHC Matters: Incorporating IHC analysis to H&E Whole Slide Image Analysis for Improved Cancer Grading via Two-stage Multimodal Bilinear Pooling Fusion

Jun Wang¹, Yu Mao¹, Yufei Cui², Nan Guan¹, and Chun Jason Xue³

¹ City University of Hong Kong
jwang699-c@my.cityu.edu.hk

² McGill University

³ Mohamed bin Zayed University of Artificial Intelligence

Abstract. Immunohistochemistry (IHC) plays a crucial role in pathology as it detects the over-expression of protein in tissue samples. However, there are still fewer machine learning model studies on IHC’s impact on accurate cancer grading. We discovered that IHC and H&E possess distinct advantages and disadvantages while possessing certain complementary qualities. Building on this observation, we developed a two-stage multi-modal bilinear model with a feature pooling module. This model aims to maximize the potential of both IHC and HE’s feature representation, resulting in improved performance compared to their individual use. Our experiments demonstrate that incorporating IHC data into machine learning models, alongside H&E stained images, leads to superior predictive results for cancer grading. The proposed framework achieves an impressive ACC higher of 0.953 on the public dataset BCI.

Keywords: Multimodal · IHC · Weakly supervised learning.

1 Introduction

Hematoxylin and eosin (H&E) is widely used in clinical practice due to its accessibility and cost-effectiveness. Recent advancements in deep learning techniques have shown promise in cancer classification, particularly in analyzing H&E whole slide images. However, analyzing these images digitally poses challenges due to their inherent characteristics. H&E-stained whole-slide images lack molecular data associated with cells and are characterized by low contrast and varying shades of dark blue and pink. These factors make it difficult for the model to efficiently learn representations during digital image analysis[8].

This limitation can be overcome by utilizing the immunohistochemistry (IHC) staining technique, which can visualize protein localization in tissue samples, aiding tumor classification and detecting small clusters of tumor cells. IHC also provides predictive and prognostic information for breast cancer. However, IHC also has some limitations.

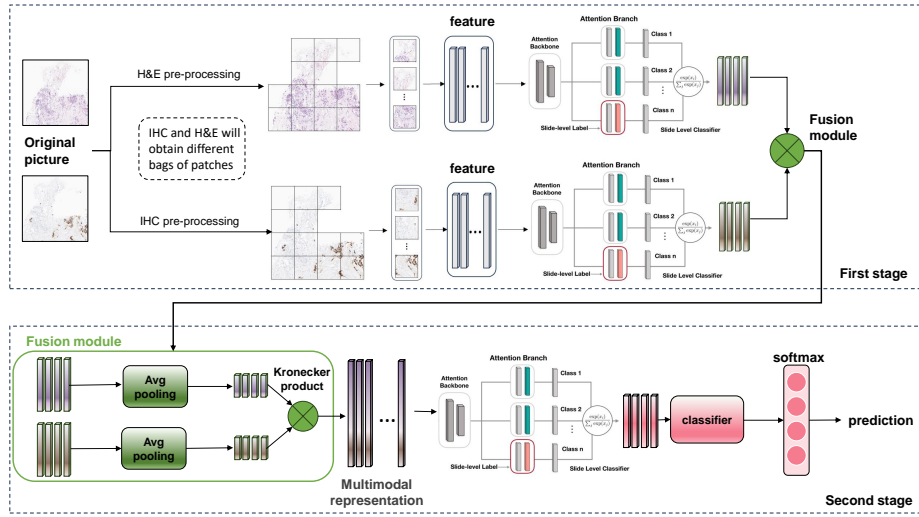


Fig. 1. Our framework: two-stage multimodal bilinear pooling Framework

The process of IHC is expensive, labor-intensive, and time-consuming compared with H&E approaches. IHC labeling requires quantifying specific positive cells or structures, not the entire image [7]. Manual determination of regions of interest (ROIs) is necessary for accurate results. However, manual annotation is subjective, time-consuming, and costly due to challenges in distinguishing different cell types and setting thresholds for classification.

We propose a two-stage multimodal bilinear pooling fusion framework to fully utilize the advantages of both H&E and IHC whole slide images. In our research, we employ Bilinear Average Pooling and Kronecker products to combine bag-level features from the H&E-based and the IHC-based pipeline. The resulting merged feature is then utilized to train the machine learning model, aiming to enhance the accuracy of cancer grading predictions. The framework is illustrated in Fig. 1. Our method achieves an accuracy score of 0.953 in breast cancer grading tasks, surpassing the performance of using either method independently. We demonstrate that combining histopathological images enhances performance and allows the model to effectively capture relevant information.

2 Related work

IHC Traditional image processing method and IHC-based machine learning focus on color vector extraction [24,21,9] and quantification of intensity features [18]. Some previous work [4,26,15] focus more on Image translation and whole-slide-image registration algorithms. They believe that it is necessary to make pixel-to-pixel matches between H&E and IHC images for further training. Also, many other work [19,2,22] think IHC dataset is hard to get so it is nec-

essary to skip IHC images and predict cancer and molecular marker only based on H&E whole slide images.

Multimodal Bilinear pooling model have been widely used in other fields for multimodal tasks. Kim et al.(2016) [12] introduce Hadamard product into the bilinear pooling model to construct the multimodal features for visual question-answering tasks. Lin et al.(2017) [14] design a bilinear layer and a pooling layer in CNN to generate features from two CNN and subsequently integrate these features via the outer product operation applied to each spatial location within the image. Many work [5,13,25] have applied multimodal technique to fusing histology and genomic multimodal data for survival prediction. However, there is no work focusing on the multimodal of the most common stains used in assessment, such as H&E and IHC, in cancer multi-class classification.

3 Method

3.1 Two-stage Multimodal bilinear pooling framework

Our framework consists of two stages, as illustrated in Fig 1. In the first stage, we employ a bilinear structure with attention-based multiple instance learning pipelines. These pipelines are trained to extract bag-level features within each modality, which are beneficial for multi-class classification prediction. Combining histopathological data from different modalities, such as H&E and IHC, poses a significant challenge due to the heterogeneity of the data. The preprocessing of WSI, specifically removing the white background, greatly impacts the training performance. Additionally, in the same pair, the preprocessed H&E image (X_{he}) may have a different bag size compared to the IHC image (X_{ihc}). However, since our training pipeline in the first stage extracts bag-level representations ($z_n \in \mathbb{R}^{1 \times 512}$) for each bag X , the bag-level representation from each modality remains the same size, regardless of any changes in the number of instances within each bag.

Once the features have been constructed from each modality, we design a fusion module to capture robust and informative inter-modality interactions between H&E and IHC features. This module constructs the new feature representations as the input of the second stage. The training pipeline in the second stage follows the same structure as the one in the first stage. We train each stage and each pipeline separately, resulting in a faster training process compared to other multimodal models in the histopathology field.

3.2 Attention-based multiple instance learning training pipeline

We first describe the whole training process for one branch and subsequently expand upon it to encompass a multi-branch structure.

The training process for a single branch Suppose we have a WSI image X , which will be denoted as "bag" in the following description. The bag X is split into K patches $X = \{x_1, x_2, \dots, x_K\}$, which is denoted as "instance". Each instance will be preprocessed and then fed into ResNet50 [10] to get the embedding. Let $R = \{r_1, r_2, \dots, r_K\}$ be the embedding result from feature extraction for bag X of K instance, $r_k \in \mathbb{R}^{1 \times 1024}$. The first fully-connected layer $W_{fc} \in \mathbb{R}^{512 \times 1024}$ compresses each embedding r_k to h_k , a denser feature vector.

$$\mathbf{h}_k = W_{fc} \mathbf{r}_k^T \in \mathbb{R}^{1 \times 512} \quad (1)$$

The denser feature vector h_k is then fed into the multi-class classification network, which consists of attention module and slide-level classifiers. Given n class, the attention network will be split into n parallel $W_{atten,1}, W_{atten,2}, \dots, W_{atten,n} \in \mathbb{R}^{1 \times 256}$. For multi-class classification, the attention module in Attention-Based MIL aggregates the set of embeddings h_k into a bag-level embedding z_n by Eq. 2, where the attention for the k -th instance is computed by Eq. 3.

$$\mathbf{z}_n = \sum_{k=1}^K a_{k,n} \mathbf{h}_k \quad (2)$$

$$a_{k,n} = \frac{\exp \{W_{atten,n}(\tanh(Vh_k^T) \odot \text{sigm}(Uh_k^T))\}}{\sum_{j=1}^K \exp \{W_{atten,n}(\tanh(Vh_j^T) \odot \text{sigm}(Uh_j^T))\}} \quad (3)$$

where $a_{k,n}$ is the confidence that k^{th} instance belongs to n^{th} class, which denoted as "attention score". $U, V \in \mathbb{R}^{256 \times 512}$ are learnable attention backbone shared for each class in the attention mechanism, and \odot is the element-wise multiplication for the gated attention mechanism. $z_n \in \mathbb{R}^{1 \times 512}$ is the weighted sum of input h_k for the n^{th} class. In this way, the input feature $R = \{r_1, r_2, \dots, r_K\}$ extracted by ResNet are encoded into a dense feature vector z_n as bag-level representation. We emphasize that the instance number in the bag would not influence the output shape of z_n , as each instance-embedding is computed with its attention score to generate the bag-level representation for the n^{th} class.

Then, for the original complete training pipeline, the bag-level representation z_n is utilized for predicting the bag-level (also called slide-level) score s_n . The bag-level score is computed by a group of classifiers $\{W_{c,1}, \dots, W_{c,n}\}$ as Eq.(4):

$$s_n = W_{c,n} z_n^T \quad (4)$$

The bag-level score s_n will be further fed into $\text{softmax}(s_n)$ for the final prediction.

Multi-branch multimodal bilinear framework The above represents a complete training pipeline for a single branch, as depicted in Fig 1. For the multimodal processing purpose, we employ two separate pipelines for H&E and IHC whole slide images in the first stage. Suppose there are M such H&E and

IHC pairs constituting the dataset $D = \{X_{he,m}, X_{ihc,m}, Y_m\}_{m=1}^M$, Y is the label of the H&E and IHC whole slide image pairs. In our paper, we extract the sets of bag representations $\{z_n\}_{m=1}^M$ for the dataset D before calculating score s_n and $\text{softmax}(s_n)$ in the first stage. We construct the sets of $\{z_{he,n}\}_{m=1}^M$ from H&E-based training pipeline and the sets of $\{z_{ihc,n}\}_{m=1}^M$ from IHC-based training pipeline, feeding into fusion module to get new feature representations of the whole H&E and IHC pair as the input of the second stage.

Loss The loss function for each independent branch is:

$$L_{total} = c_1 L_{slide} + c_2 L_{patch} \quad (5)$$

where L_{slide} is compared with the ground truth by cross-entropy loss and L_{patch} is the binary smooth SVM loss between the pseudo label generated for top-k patches with the inference of instance-level classifier.

3.3 Fusion Module

We are motivated to pursue multimodal learning because we believe that the interaction between H&E and IHC image features will enhance the accuracy of predicting cancer grading. In our previous training pipeline, we created two bag-level feature representations. Now, our goal is to explicitly capture the significant pairwise feature interactions through a fusion module.

Bilinear Average Pooling The initial Bilinear pooling mechanism [12] was introduced to merge features obtained from two distinct CNNs, both trained on the same image, in order to improve fine-grained visual recognition. The scenario discussed in this paper bears resemblance to the aforementioned situation. As stated earlier, we utilize X_{he} and X_{ihc} as our inputs, representing different staining techniques applied to cells at identical locations, resulting in distinct feature representations of the same sample. Therefore, at this stage, we employ bilinear pooling to fuse these features together.

In contrast to the original Bilinear pooling mechanism [12], which utilizes element-wise product and sum-pooling, our approach employs an average pooling σ for bilinear pooling. This is done to reduce the size of the feature space and facilitate the fusion of bilinear features. In the first stage, when dealing with the features $z_{he,n}$ and $z_{ihc,n}$ from the bilinear pipeline, direct convolution fusion is not suitable due to the high dimensionality of these features. By employing average pooling σ , we are able to compress the dimensions of $z_{he,n}$ and $z_{ihc,n}$ from 512 to 32. Subsequently, these compressed features are fused using the Kronecker product.

Kronecker product The original method proposed by [12] utilizes element-wise products to combine features in the Bilinear pooling mechanism. In histopathology, previous research [6,5] has explored various forms of the Kronecker product

to fuse histology or genomics features. In other multimodal studies on cancer prognosis prediction, researchers have employed direct feature combination [11] or score-level fusion [20] to integrate data from different modalities. However, these approaches may not adequately capture the intricate relationships between modalities.

We utilize the Kronecker product for feature fusion. Consider there are two matrices, $A \in \mathbb{R}^{m \times n}$ and $B \in \mathbb{R}^{l \times p}$. The Kronecker product, denoted as \otimes , is an operation that combines these matrices into a block structure, determined by the elements of the original matrices.

$$A \otimes B = \begin{bmatrix} a_{11}B & \cdots & a_{1n}B \\ \vdots & \ddots & \vdots \\ a_{m1}B & \cdots & a_{mn}B \end{bmatrix}$$

Therefore, the joint multimodal tensor constructed from the Kronecker product, as shown in Eq.(6), will capture the important bi-modal interactions that characterize both modalities.

$$F = \sigma(z_{he,n}) \otimes \sigma(z_{ihc,n}) \quad (6)$$

Upon constructing this joint representation, we utilize the multi-modal representation F as input. We then proceed to learn the representation through the previous training pipeline [16], and subsequently train it using cross-entropy loss for cancer grading tasks. The ultimate significance of pathological fusion lies in its ability to combine diverse patterns and improve prediction accuracy.

4 Experiments

4.1 Datasets

We use two public breast cancer datasets in this paper. BCI dataset [15] presents 4870 registered H&E and IHC pairs, covering a variety of HER2 expression levels from 0 to 3. IHC4BC dataset [1] contains H&E and IHC pairs in ER and PR breast cancer assessment, and categories are defined ranges 0 to 3 respectively. The number of each subset is 26135 and 24972.

4.2 Implementation Details

We use CLAM [16] pre-processing tools to create patches and extract features from each WSI image. Some WSIs will be dropped due to the segment and filtering of CLAM pre-processing mechanism, we take the intersection of H&E and IHC pre-processed WSIs for further training. The learning rate of Adam optimizer is set to 2×10^{-4} , the weight decay is set to 1×10^{-5} , the early-stop strategy is used and the max training epochs is 200. We evaluate our method in two datasets for breast cancer grading tasks with 5-fold Monte Carlo cross-validation. For each cross-validated fold, we randomly split each dataset into 80%-10%-10% subset of training, validation, and testing, stratified by each class.

4.3 Results

In this section, We compared our framework with the following methods frequently used in supervised and weakly supervised learning to test our model’s prediction performance and robustness. Accuracy(ACC) and Area under the ROC Curve (AUC) are selected as evaluation metrics.

Table 1 illustrated the results of our model compared with other models in BCI dataset.

Table 1. Experiment results on BCI dataset.

Model	image type	AUC	ACC
InceptionV3	H&E	0.8233	0.804
Resnet	H&E	0.8857	0.872
Vit [3]	H&E	0.92	0.904
IHCNet [23]	IHC	-	0.9345
DenseNet	H&E	0.89	0.68
HE-HER2Net [22]	H&E	0.98	0.87
convoHER2[17]	H&E	-	0.851
convoHER2	IHC	-	0.878
CLAM [16]	H&E	0.987	0.909
CLAM	IHC	0.991	0.917
Two-Stage Multimodal Bilinear Fusion(ours)	H&E and IHC	0.996	0.953

As shown in Table 1, our two-stage bilinear fusion framework outperformed all other existing models, achieving an impressive AUC of 0.996 and ACC of 0.953. Our model achieved a remarkable AUC score close to 1, indicating its strong classification ability among multiple classes. Hence, our proposed model exhibited exceptional performance in the multi-class classification task.

We also conducted experiments on the IHC4BC-ER and -PR datasets to test our motivation and methods. Our findings demonstrate that IHC-based machine model performs better than H&E-based model. Specifically, our two-stage bilinear fusion framework achieves a higher ACC compared to both H&E-based and IHC-based models in the IHC4BC dataset.

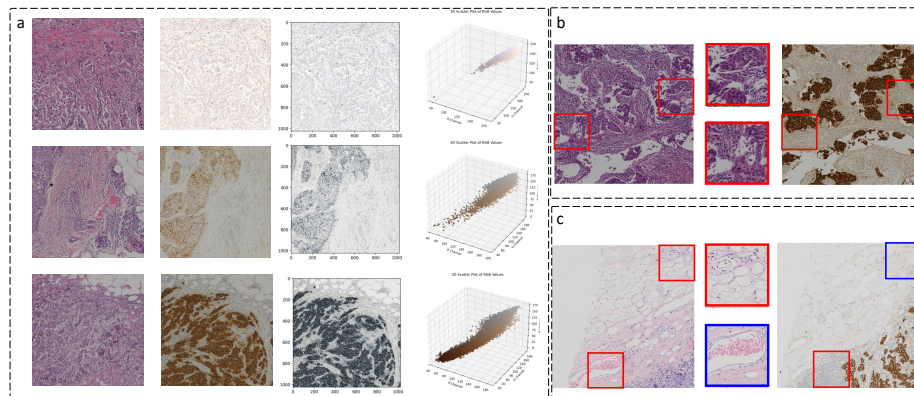
4.4 Discussion

In this section, we analyze the wrong prediction of each model and derive two key insights:

IHC medical images have inherent characteristics in color and morphology The H&E WSIs depicted in Fig. 2 (a) exhibit incorrect predictions, contrasting with the accurately predicted paired IHC WSIs. The third column illustrates the IHC staining level related to the grade of the WSI by color deconvolution. The fourth column presents a 3D scatter plot of optical density RGB values. These observations underscore the color characteristics in IHC images enabling the IHC-based model to learn representation well.

Table 2. Experiment results on IHC4BC dataset.

Model	image type	IHC4BC-ER		IHC4BC-PR	
		AUC	ACC	AUC	ACC
CLAM	H&E	0.9543	0.8421	0.9089	0.7734
CLAM	IHC	0.9796	0.8941	0.9609	0.847
Two-Stage Multimodal Bilinear Fusion(ours)	H&E and IHC	0.981	0.905	0.9621	0.8482

**Fig. 2.** H&E-based machine learning the wrong prediction. However, for their paired IHC images, there are huge differences in color and can be identified correctly in the IHC-training pipeline.

H&E-based model learn wrong high attention area or can't learn the right area well H&E-based models allocate top-k attention correctly but struggle to extract meaningful representations from H&E images. The CLAM model, using clustering and attention-based MIL mechanism, sometimes allocates the highest top-k attention correctly but still makes wrong predictions. Additionally, in Fig. 2 (c), the trained model allocates the highest top-k attention to erroneous areas, as evidenced by the zoom-in patch in the blue box. These areas contain fewer staining cells with brown hues in the paired IHC image, leading to inaccurate predictions.

5 Conclusion

We present a novel two-stage multimodal bilinear pooling fusion framework, designed for integrating both H&E as well as IHC whole slide images into cancer grading tasks. Our experiments on the publicly available BCI dataset

demonstrate that our framework achieves state-of-the-art performance. The outcomes of our study underscore the efficacy of employing multimodal features in histopathological tasks, resulting in enhanced performance metrics. Moreover, our experiments reveal that aligning IHC datasets with H&E at the pixel level is unnecessary.

References

1. Akbarnejad, A., Ray, N., Barnes, P.J., Bigras, G.: Predicting ki67, er, pr, and her2 statuses from h&e-stained breast cancer images. arXiv preprint arXiv:2308.01982 (2023)
2. Anand, D., Yashashwi, K., Kumar, N., Rane, S., Gann, P.H., Sethi, A.: Weakly supervised learning on unannotated h&e-stained slides predicts braf mutation in thyroid cancer with high accuracy. *The Journal of pathology* **255**(3), 232–242 (2021)
3. Ayana, G., Lee, E., Choe, S.w.: Vision transformers for breast cancer human epidermal growth factor receptor 2 expression staging without immunohistochemical staining. *The American Journal of Pathology* (2023)
4. Bai, B., Yang, X., Li, Y., Zhang, Y., Pillar, N., Ozcan, A.: Deep learning-enabled virtual histological staining of biological samples. *Light: Science & Applications* **12**(1), 57 (2023)
5. Chen, R.J., Lu, M.Y., Wang, J., Williamson, D.F., Rodig, S.J., Lindeman, N.I., Mahmood, F.: Pathomic fusion: an integrated framework for fusing histopathology and genomic features for cancer diagnosis and prognosis. *IEEE Transactions on Medical Imaging* **41**(4), 757–770 (2020)
6. Chen, R.J., Lu, M.Y., Williamson, D.F., Chen, T.Y., Lipkova, J., Noor, Z., Shaban, M., Shady, M., Williams, M., Joo, B., et al.: Pan-cancer integrative histology-genomic analysis via multimodal deep learning. *Cancer Cell* **40**(8), 865–878 (2022)
7. Cizkova, K., Foltynkova, T., Gachechiladze, M., Tauber, Z.: Comparative analysis of immunohistochemical staining intensity determined by light microscopy, imagej and qpath in placental hofbauer cells. *Acta histochemica et cytochemica* **54**(1), 21–29 (2021)
8. Dimitriou, N., Arandjelović, O., Caie, P.D.: Deep learning for whole slide image analysis: an overview. *Frontiers in medicine* **6**, 264 (2019)
9. Geread, R.S., Morreale, P., Dony, R.D., Brouwer, E., Wood, G.A., Androutsos, D., Khademi, A.: Ihc color histograms for unsupervised ki67 proliferation index calculation. *Frontiers in bioengineering and biotechnology* **7**, 226 (2019)
10. He, K., Zhang, X., Ren, S., Sun, J.: Deep residual learning for image recognition. In: *Proceedings of the IEEE conference on computer vision and pattern recognition*. pp. 770–778 (2016)
11. Huang, Z., Zhan, X., Xiang, S., Johnson, T.S., Helm, B., Yu, C.Y., Zhang, J., Salama, P., Rizkalla, M., Han, Z., et al.: Salmon: survival analysis learning with multi-omics neural networks on breast cancer. *Frontiers in genetics* **10**, 166 (2019)
12. Kim, J.H., On, K.W., Lim, W., Kim, J., Ha, J.W., Zhang, B.T.: Hadamard product for low-rank bilinear pooling. arXiv preprint arXiv:1610.04325 (2016)
13. Li, R., Wu, X., Li, A., Wang, M.: Hfbsurv: hierarchical multimodal fusion with factorized bilinear models for cancer survival prediction. *Bioinformatics* **38**(9), 2587–2594 (2022)
14. Lin, T.Y., RoyChowdhury, A., Maji, S.: Bilinear cnn models for fine-grained visual recognition. In: *Proceedings of the IEEE international conference on computer vision*. pp. 1449–1457 (2015)

15. Liu, S., Zhu, C., Xu, F., Jia, X., Shi, Z., Jin, M.: Bci: Breast cancer immunohistochemical image generation through pyramid pix2pix. In: Proceedings of the IEEE/CVF Conference on Computer Vision and Pattern Recognition (CVPR) Workshops. pp. 1815–1824 (June 2022)
16. Lu, M.Y., Williamson, D.F., Chen, T.Y., Chen, R.J., Barbieri, M., Mahmood, F.: Data-efficient and weakly supervised computational pathology on whole-slide images. *Nature biomedical engineering* **5**(6), 555–570 (2021)
17. Mridha, M., Morol, M.K., Ali, M.A., Shovon, M.S.H.: convoher2: A deep neural network for multi-stage classification of her2 breast cancer. arXiv preprint arXiv:2211.10690 (2022)
18. Mukundan, R.: Analysis of image feature characteristics for automated scoring of her2 in histology slides. *Journal of Imaging* **5**(3), 35 (2019)
19. Naik, N., Madani, A., Esteva, A., Keskar, N.S., Press, M.F., Ruderman, D., Agus, D.B., Socher, R.: Deep learning-enabled breast cancer hormonal receptor status determination from base-level h&e stains. *Nature communications* **11**(1), 1–8 (2020)
20. Sahasrabudhe, M., Sujobert, P., Zacharaki, E.I., Maurin, E., Grange, B., Jallades, L., Paragios, N., Vakalopoulou, M.: Deep multi-instance learning using multi-modal data for diagnosis of lymphocytosis. *IEEE Journal of Biomedical and Health Informatics* **25**(6), 2125–2136 (2020)
21. Shi, P., Zhong, J., Hong, J., Huang, R., Wang, K., Chen, Y.: Automated ki-67 quantification of immunohistochemical staining image of human nasopharyngeal carcinoma xenografts. *Scientific reports* **6**(1), 32127 (2016)
22. Shovon, M.S.H., Islam, M.J., Nabil, M.N.A.K., Molla, M.M., Jony, A.I., Mridha, M.: Strategies for enhancing the multi-stage classification performances of her2 breast cancer from hematoxylin and eosin images. *Diagnostics* **12**(11), 2825 (2022)
23. Shovon, M.S.H., Shin, J., Mridha, M.: Ihcnet: Advancing multi-stage her2 status detection in breast cancer using interpretable robust transfer learning model from ihc images. In: 2023 International Conference on Innovation and Intelligence for Informatics, Computing, and Technologies (3ICT). pp. 326–332. IEEE (2023)
24. Van Eycke, Y.R., Allard, J., Salmon, I., Debeir, O., Decaestecker, C.: Image processing in digital pathology: an opportunity to solve inter-batch variability of immunohistochemical staining. *Scientific reports* **7**(1), 42964 (2017)
25. Wang, Z., Li, R., Wang, M., Li, A.: Gpdbn: deep bilinear network integrating both genomic data and pathological images for breast cancer prognosis prediction. *Bioinformatics* **37**(18), 2963–2970 (2021)
26. Weitz, P., Valkonen, M., Solorzano, L., Carr, C., Kartasalo, K., Boissin, C., Koivukoski, S., Kuusela, A., Rasic, D., Feng, Y., et al.: A multi-stain breast cancer histological whole-slide-image data set from routine diagnostics. *Scientific Data* **10**(1), 562 (2023)